Examination of temperature distribution on silicon nitride engineering ceramics during fibre laser surface treatment

Shukla, P. & Lawrence, J.

Original citation & hyperlink:
Shukla, P & Lawrence, J 2011, 'Examination of temperature distribution on silicon nitride engineering ceramics during fibre laser surface treatment' Optics and Lasers in Engineering, vol. 49, no. 7, pp. 998–1011.
https://dx.doi.org/10.1016/j.optlaseng.2011.01.014

DOI 10.1016/j.optlaseng.2011.01.014
ISSN 0143-8166

Publisher: Elsevier

Examination of Temperature Distribution and the Thermal Effects on Si_3N_4 Engineering Ceramics during Fibre Laser Surface Treatment

P. P. Shukla* and J. Lawrence [Ψ]

Corresponding Author's Details:

Pratik P. Shukla*,

Loughborough University,

Wolfson School of Mechanical and Manufacturing Engineering,

Leicestershire,

LE11 3TU,

United Kingdom,

Email: P.Shukla@lboro.ac.uk,

Direct Line: +44 (0) 1509227592

Second Author's Details:

Jonathan Lawrence [Ψ]

Lincoln School of Engineering,

University of Lincoln,

Brayford Pool,

Lincoln,

LN6 7TS,

United Kingdom

Abstract

The thermal effects of fibre laser surface treatment on a Si_3N_4 engineering ceramic were studied using a computational finite element analysis (FEA) model. Temperature increases on the surface of the Si_3N_4 during fibre laser processing were measured using an infra-red thermometer; temperature distributions in the bulk were measured with specifically located thermocouples. A computational model using FEA was then developed to model the flow and the distribution of the radiated heat resulting from the fibre laser treatment of the Si_3N_4 ceramic. By utilizing data obtained from a TG-DSC analysis the FEA model predictions of the temperature distribution were used to map phase transformations and significant events occurring during the fibre laser surface treatment of the Si_3N_4. This study revealed that the fibre laser surface treatment generally resulted in a phase transformation of the Si_3N_4 from α-phase to β-phase modification and refinement in the grain boundary phase as various changes were found with grain size, shape and its direction after the fibre laser surface treatment of the Si_3N_4 ceramic.

Keywords: Fibre laser, Si_3N_4, engineering ceramics, FEA, Phase transformation.

1. Introduction

Laser surface treatment in general is a complex process particularly with engineering ceramics due to the involvement of multi-parameters such as power density; traverse speed; instantaneous heating; ablation; rapid cooling and solidification. Evaluation of such a process can be conducted by means of employing an experimental, analytical and computation approaches to investigate the laser-ceramic surface interaction.

Prior investigations by many workers has demonstrated methods of predicting and calculating the surface and the bulk temperature of various laser processing methods by using numerical means. Cline and Anthony [1] carried out one of the first investigations to determine the temperature of a metallic alloy during CO_2 laser processing. Analytical model was adopted by using the Greens's function for a Gaussian laser beam which was traversing at a constant velocity. Lax [2, 3] investigated a one-dimensional numerical integral of a solid material by the temperature rise during an onset of a Gaussian laser beam when applying a steady-state solution and by taking in account of the constant and the temperature-dependent thermo-physical properties for the solid. Nissim *et al.* [4] also employed the Greens's function to calculate temperature profiles of an elliptical laser beam during annealing of a silicon gallium arsenide (semiconductor). The results showed that with prior knowledge of the thermal conductivity, accurate temperature can be calculated and are valid for any material. Moody & Handel [5] also employed a CW (continuous wave) elliptical laser beam by using an improved formula of the Kirchhoff transformation and elucidated the temperature profiles on a silicon substrate. Thermal conductivity, diffusivity, and the surface reflection were considered as important

functions in the analysis. Their findings showed variation in the temperature profiles within the molten, the semi liquid and the solid regions.

Kar & Mazumber [6] implemented the three-dimensional (3-D) transient heat conduction equation to generate temperature predictions as well as a FEM of a Gaussian laser beam chemical vapour deposition process thereof on a pure titanium work-piece. This showed a relationship between the variation in the temperatures at fluctuating laser powers and the traverse speeds. Kar *et al.* [7] then followed an investigation using a quasi-steady-state heat conduction model to analyse the laser heating of a solid substrate with rectangular, square, multimode, and single or multiple laser beams which showed approximation of the temperature spread during the laser heating with a single or multiple beams by using a rectangular spots.

A computational and an experimental model were rather adopted in this study as opposed to a numerical model for calculating the temperature distribution. This was due to simplicity, to obtain accuracy and also because it is less time consuming especially with the adopting the computational FEM technique. The temperature measurement by adopting the experimental approach would also aid in obtaining realistic test results in comparison to a analytical model which does not consider the physical aspects such as the heat transfer from the work-piece to the clamps or the processing table (as a second body) in contact with the test-piece. This significantly effects the temperature distribution as opposed to a finite body in space used without any constraints in the analytical models.

Experimental measurement of the laser processing temperatures can be difficult with hard, brittle engineering ceramics and often requires a tedious and lengthy preparation as holes are required to be drilled within the ceramic for mounting the temperature sensors or thermocouples. But this method is generally adopted for measuring the temperature changes in the bulk; it is not suitable for measuring the surface temperatures. Therefore, a pyrometers or contact-less devices are useful for measuring the temperature on the surface and was as demonstrated by Zhang *et al.* [8], Hao & Lawrence [9] and Ignatiev *et al.* [10]. Ignatiev *et al.* also stated that such measuring techniques are helpful to detect the material's phase transformation. The investigation herein also adopted this approach as the experimentally measured temperatures are used as an input parameter into the computational models to elucidate the thermal heat map and the heat distribution.

The use of finite element analysis (FEA) has been demonstrated by several studies by using design software such as ABACUS and ANSYS for investigating the residual stress and the thermal distribution of various laser processing technique applied on conventionally used metals and alloys. Braisted & Brockman [11], Yongxiang *et al.* [12], Ocana *et al.* [13], Chen *et al.* [14] who studied the laser surface treatment through shock peening and constructed a 3-D model of the process which led to the determination of residual stress fields and surface deformation. Kim [15] studied the steady heat transfer equation to model the evaporating laser cutting process using a 3-D computational finite element model. Shiomi *et al.* [16] analysed a laser rapid prototyping of metallic powders with the aid of a FEA. Investigation of the temperature fields and the stress state during laser welding by the aid of a simulated FEM and the thermal heat map produced to improve the laser welding process was

conducted by Carmingnani *et al.* [17]; Spina *et al.* [18]; Yilbas *et al.* [19]; Zain-Ul-Abdein *et al.* [20] and Naeem *et al.* [21]. Much work has been conducted with modelling various laser processes with metals; however, very little work has been published with finite element modelling of laser surface treatment of engineering ceramics.

Considerable amount of research has also been conducted within the field of phase transformation of the Si_3N_4 ceramics [22-29]. The phase transformation of the Si_3N_4 ceramic occurs when it is exposed to changing temperatures. With respect to the changing temperature being introduced during the laser surface treatment; it is important to understand the thermal effects of the laser radiation upon various phase changes within the Si_3N_4 ceramic. Phase transformation of the Si_3N_4 ceramic during laser surface processing is however, unreported in the literature. Phase transformation of Si_3N_4 ceramics is complex in comparison to other ceramics such as a ZrO_2. This is because the behaviour of the Si_3N_4 during the heating process involves considerable densification via particle arrangement, solution diffusion-precipitation and coalescence which are all required for a full α-phase to β-phase conversion [22].

Messier *et al.* [23] investigated the phase transformation of powder Si_3N_4 and reported that a change of α-phase to β-phase occur at 1600 ◦C. Effect of this transition also leads to formation of fine log-shaped grains with hexagonal symmetry are formed. Messier *et al.* also stated that α-phase was generally formed at low temperature. Ziegler and Hasselman [24] investigated the phase transformation of hot pressed Si_3N_4 (HPSN) and reaction sintered Si_3N_4 (RSSN) ceramic and reported that different morphology is formed with change in phase with respect to the increase in

the temperature. The *β*-phase grain structure has the tendency to comprise of a rod like grains which are formed at about 1499 ◦C. Sarin [22] also commented on the increased grain size of the ceramics and occurrence of wiskar rod-type grains with high aspect ratio forming at 1880 ◦C during sintering of the ceramic for 4 hours. Formation of the rod-like grains and transition to *β*-phase was also confirmed by the work of Sajgalik and Galusek [25]. Rouxel *et al.* [26] reported a phase transformation of the Si_3N_4 ceramic from *α*-phase to *β*-phase occur between sintering temperatures of 1549 ◦C to 1649 ◦C. Increase in the fracture toughness via decrease in the hardness and the Young's modulus was also reported in Rouxel *et al.*'s investigation which all occurred through micro-structural changes that are found in the work of previous researchers. Yang *at al.* [27] also investigated the change in phases occurring with the Si_3N_4-MgO-CeO_2 ceramic and found that densification of the ceramic occurs at 1500 ◦C which is followed by the phase transition of the Si_3N_4-MgO-CeO_2 from *α*-to-*β* arising at 1500 ◦C and ending at 1600 ◦C.

Dai *et al.* [28] conducted an in depth study of the phase transformation behaviour of the Si_3N_4 at temperature between 1600 ◦C to 1800 ◦C. It was reported that *α*-to-*β* transformation occurred when heating the ceramic to 1600 ◦C. This finding also complied with the finding of Jiang *et al*. [29] and the work of various authors reviewed previously. Dai *et al.* also reported that SiO_2 was formed during the *α*-phase to *β*-phase transition which has already been seen by the work of Shukla and Lawrence [30] who investigated the characterization of Si_3N_4 engineering ceramics by means fibre laser radiation.

This research attempts to look at the underlying effects during such phase changes and how the Si_3N_4 engineering ceramic is evolved from the fibre laser radiation. Thermal distribution and the change in the Si_3N_4 characteristics during the fibre laser surface treatment were under investigation. This was done by performing an experimental investigation of the temperature exhibited during the fibre laser radiation within the bulk and the surface of the Si_3N_4 ceramics. Consequently, mapping of the heat distribution within Si_3N_4 engineering ceramics by an experimental model and by using a finite element model (FEM) with the aid of Unigraphics NX 5 Nastran design and simulation software by Sham [31] is presented herein. In addition, verification of the experimental model in comparison to the FEM; phase transformation within the Si_3N_4 was speculated at various temperatures prior to, during and after the fibre laser surface treatment of the Si_3N_4 engineering ceramics. The experimental values were used as the input parameter for constructing an FEM which is then used for postulating any changes within the Si_3N_4 ceramic, through data obtained from a thermo, gravimetry- differential scanning calorimetry (TG-DSC).

2 Development of the fibre laser surface treatment of the Si_3N_4 ceramic

2.1 Thermal modelling

It is important to study the event during the fibre laser interaction with the Si_3N_4 ceramic. The fibre laser with a given power density and a constant traverse speed (see section 3.2) is passed on the top surface of the Si_3N_4 ceramic. During this instance the laser energy is absorbed by the ceramic to about 90% as reported by Zhang and Modest [8]. The absorbed light in form of heat causes a degree of surface heating which leads to a degree of melting, followed by some level of ablation through

vaporization and finally solidifies during its cooling process to ambient temperatures. Phase changes during such events also occur at certain temperature gradients as mentioned earlier in this study. Furthermore, an analytical solution as presented in equation 2.1 onwards can be adopted to evaluate an analytical model.

$$\partial^2 (k\theta)/ \partial x^2 + \partial^2 (k\theta)/ \partial y^2 + \partial^2 (k\theta)/ \partial z^2 + qb = \rho c_p \partial\theta/\partial t \quad (2.1)$$

Where θ is the temperature and k_{ij} are the conductivity co-efficient. The variable ρ, c_p and q_b are mass density, the specific heat and the rate of heat generation per unit volume. The thermal energy acting on the surface of the Si_3N_4 ceramic due to convection to the environment is governed by

$$q = - h (\theta - \theta^0), \quad (2.2)$$

where q is the heat energy across the surface, h is a reference film co-efficient, θ is the temperature at this point on the surface and θ^0 is a reference temperature value. The thermal energy on a the Si_3N_4 ceramic is due to radiation to the environment and is governed by

$$q = A [(\theta - \theta^Z)^4 - (\theta^0 - \theta^Z)^4], \quad (2.3)$$

where q is the thermal energy across the surface of the Si_3N_4 ceramic, A is the radiation constant, θ is the temperature at this point on the surface, θ^0 is an ambient temperature value and θ^Z is the value of absolute zero on the temperature scale being used. Therefore, the radiation constant is defined as:

$$A = \varepsilon\sigma, \quad (2.4)$$

Where ε is the emissivity of the surface and the σ is the Stefan Boltzmann constant. In a situation where phase change occurs, particularly so for a pure substance, then the following boundary conditions of Rolph and Bathe [31] is applied at the phase transition interface at the solid-liquid interface:

$$\theta = \theta_f, \tag{2.5}$$

$$\Delta q_S \, dS = -\rho L \, dV/dt \tag{2.6}$$

where θ_f, ρ and L are the phase change temperatures, mass density and latent heat per unit mass of the material undergoing phase change and V is the volume. The heat is absorbed at a rate proportional to the volumetric rate of conversion of the material, dV/dt, at the solid liquid interface as stated by Equation (2.6). The heat must also be balanced by the heat flow, Δq_s, from the interface. The –ve sign is used for a situation where absorption of heat during melting occurs. The steps to construct the FEM by using a computational method of steady state solution are further presented with its 3-D geometry.

2.2 FEM development

A FEM was constructed using Unigraphics, NX 5.0, Nastran design software which included several steps for its construction and is presented in Figure 1. The model was prepared to demonstrate the thermal distribution of the fibre laser radiated heat which is then compared to the experimental heat distribution model to investigate if there is a correlation between the two methods.

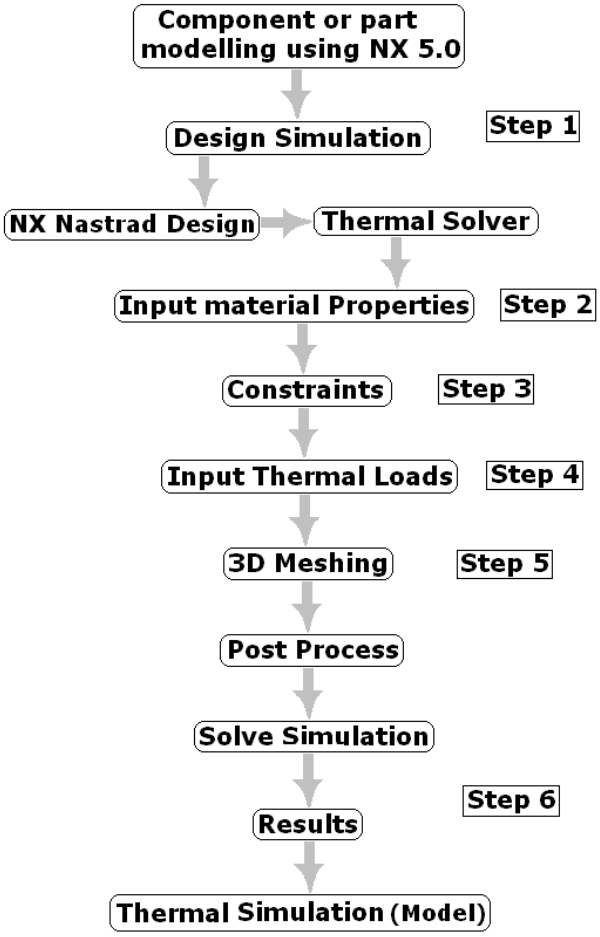

Figure 1 A schematic diagram of the steps taken to construct the FEM of the fibre laser radiated surface of the Si_3N_4 engineering ceramic.

The component part was first designed which represented the experimental work-piece (see Figure 2). It comprised of a diameter of 3mm diameter blind hole with a depth of 100μm, equivalent to the foot-print of the fibre laser beam. A depth of 100μm was assigned for the blind hole as it was found from a previous investigation by Shukla and Lawrence [33, 34] that the average laser beam penetration on the ceramic was about 100μm in depth. It was necessary to introduce the blind hole to the model to assign a heat load acting on the work-piece as opposed to assigning the laser beam as a heat load since the laser beam is not a solid object and does not have the required physical properties for the model to function correctly. This also helped to minimize the computational time and the model complexity during the simulation.

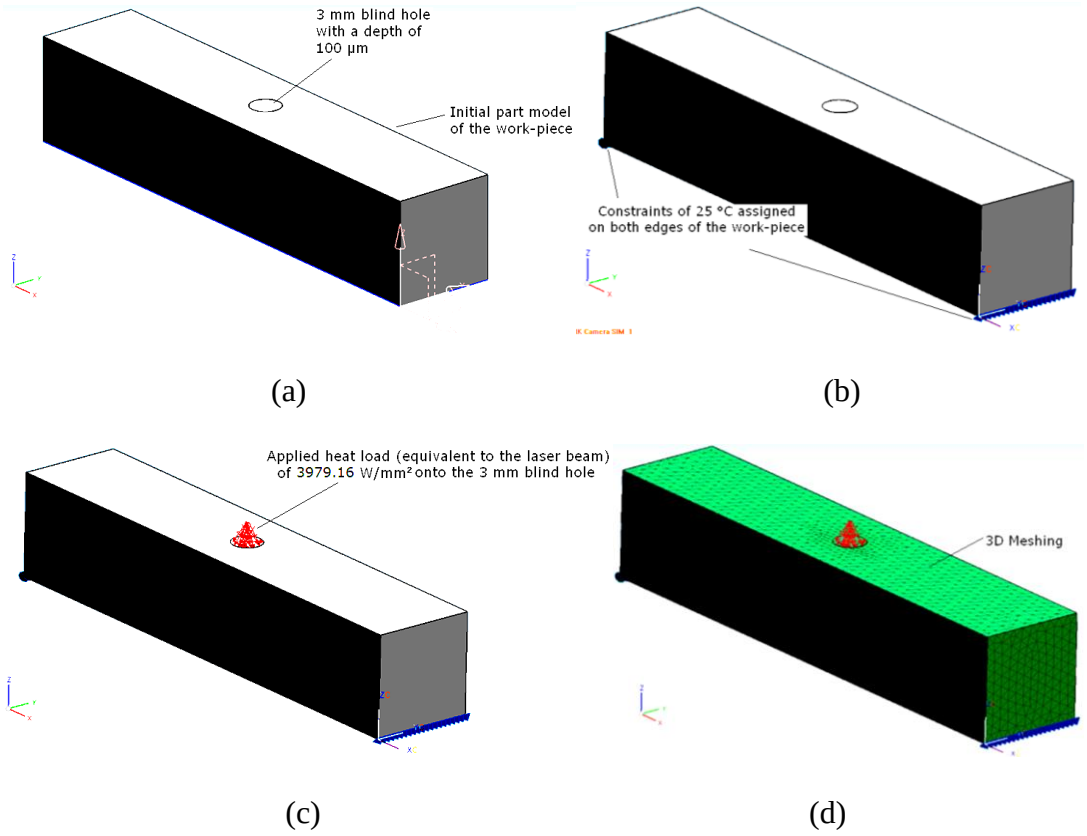

Figure 2 Screen shot images of the part design showing a 3mm diameter blind hole at a depth of 100µm in (a), the thermal constraint of 25°C applied on both edges to the work-piece in (b), application of the heat load to the work-piece in form of the laser beam in (c) and (d); an image of the full 3-D mesh showing the assigned heat load to the Si_3N_4 engineering ceramic.

The second step to construct the model was to assign the material properties. However, the user must ensure that the correct software functions are selected, namely: the design simulation followed by NX Nastrad design and the thermal solver. The materials properties are presented in Table 1 and were then assigned to the work-piece. Young's modulus; Poisson's ration; shear modulus; thermal expansion coefficient and the thermal conductivity are predominant properties directly affecting the model and hence, were assigned in all three X-Y and Z directions using the orthotropic material function of the NX Nastrad design, (thermal solver). This was

because the characteristic of the ceramic does not remain the same in all axis of its orientations as shown in the previous research by Shukla and Lawrence [34].

Table 1 Input of the properties assigned to the Si_3N_4 engineering ceramic to construct the FEM.

Material Properties	Value
Mass Density	3200 kg/m^3
Reference Temperature	25 °C
Specific Heat	900 J/kg-k
Young's Modulus	320000 MPa
Poisson's Ratio	0.27
Shear Modulus	110000 MPa
Thermal Expansion Coefficient	3.25 u /°C
Thermal Conductivity	15 W/m-k

After assigning the material properties, the third step of the FEA was to give constraints to the work-piece. The constraint is in form of a thermal constraint and is assigned to the work-piece in positions where the sample is connected to another body (i.e mounted to the processing table by using putty). A putty was used since mechanical clamping is not always ideal for holding hard brittle ceramics due to the risk of as inducing a mechanical tensile stress which often leads propagation of fractures. Furthermore the use of putty provided a firm fixation and avoided vibrations when the working table was in motion during the fibre laser processing. A thermal constraint of 25 °C was applied to the positions shown in Figure 2(b) on both edges of the work-piece. This meant that the work-piece was held firm in those positions and was in contact with another body during the fibre laser processing. The temperature of the thermal constraint was applied at an atmospheric temperature of 25 °C.

Step four of the FEA involved applying a heat load to the work-piece. This is where a heat load of 2269 °C found from the experimental work was applied on the 3 mm diameter blind hole (see Figure 2(c)) on the work-piece at the laser power density of 3979.16 W/mm^2. This was the maximum power density induced by the 3mm diameter beam of the fibre laser. The surface of the Si_3N_4 was assigned a view factor of 1. This is the amount of or heat being passed on from one surface to another; in this case, the thermal energy radiated by the laser beam was only being passed onto one surface during the heat transfer [35]. Absorption of 90 % was assigned to the model by taking in consideration of the absorption values found in a previous investigation by Zhang & Modest [8]. An emissivity of 0.40 was used as it is a typical value for all ceramics.

Once a thermal load was applied the FEM is then ready to be meshed. Furthermore, a fine 3-D mesh of tetrahedral using 10 nodes, with an overall element size of 1 was created on the work-piece as is presented in Figure 2 (d). The final step of the FEA is to create a simulation using the post processing function of the NX 5.0 Nastran software. This generated a solution from the input data and produced a simulation in form of a FEM which was also animated to investigate the distribution of heat during prior to, during and after the laser process.

3. Experimental Techniques and Analysis

3.1. Experimental material

The material used for the experimentation was cold isostatic pressed (CIP) Si_3N_4 with 90% Si_3N_4, 4% Yttria, 4% Al_2O_3 and 2% other, unspecified content by the manufacturer (Tensky International Company, Ltd.). Each test piece was obtained in a

bulk of 10 x 10 x 50 mm^3 with a surface roughness of 1.56 μm (as-received from the manufacturer). This was to reduce the laser beam reflection as the well polished shinier surfaces of the ceramic would reduce beam absorption. The experiments were conducted in ambient condition at a known atmospheric temperature (20°C). All surfaces of both the Si_3N_4 engineering ceramic to be treated were marked with black ink prior to the fibre laser surface treatment to enhance the absorption and allow the laser beam to further penetrate into the surface. Initial experiments reviewed that the black ink helped the beam to absorb better into the material. The back ink was generally removed by the fibre laser surface treatment and was not found to have any further effect on the ceramics after the laser surface interaction had taken place.

3.2. Fibre laser surface treatment

A 200 W fibre laser (SP-200c-002; SPI, Ltd.) as shown in Figure 3 which emitting a continuous wave (CW) mode beam at a wavelength of 1.075μm was used for this work. Focal position was kept to 20 mm above the work-piece to obtain a 3 mm spot size. The processing gas used was compressed air as well as ambient air supplied at a flow rate of 25 litre per min. Programming of the laser was conducted by using SPI software, which integrated with the fibre laser system. A 50 mm line was programmed using numerical control (NC) programming as a potential beam path which was transferred by .dxf file. To obtain an operating window, trials were conducted at the fixed spot size of 3 mm and by varying the power between 75 and 200 W and varying the traverse speed between 25 and 500 mm/min. From these trials it was found that 143.25 W at 100 mm/min were the ideal laser parameter to use in terms of achieving a crack-free surface.

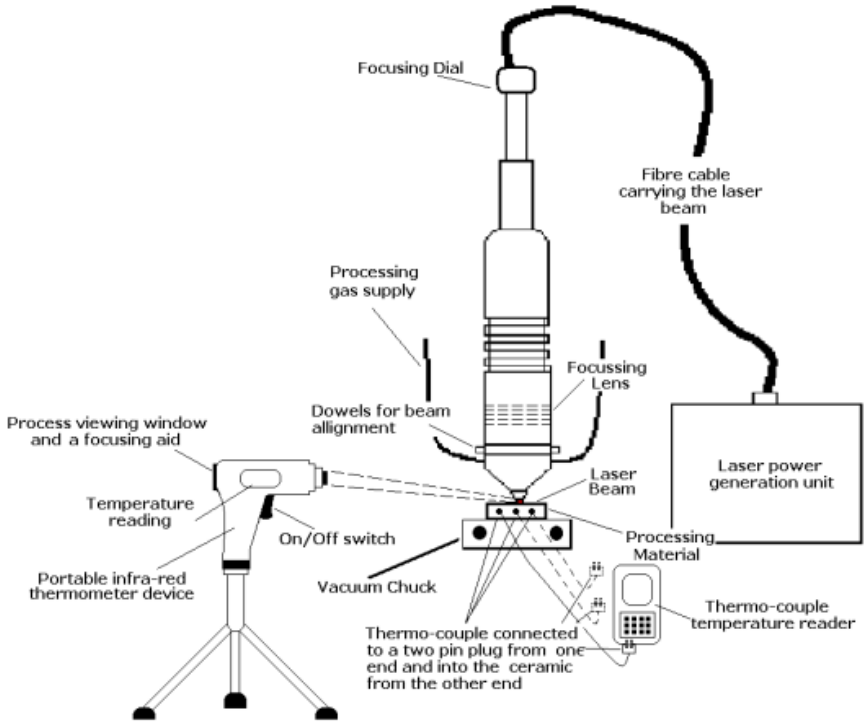

Figure 3 Schematic diagram of the experimental set-up of the fibre laser processing of the Si_3N_4 engineering ceramic.

3.3. Temperature Measurements

3.3.1. Infra-red thermometer

The surface processing temperature was measured by using a portable infra-red thermometer (Cyclops 100 B; Land instruments international Ltd). The device was bolted on a tripod and positioned 1 m away from the processing area (see Figure 3). The infra-red thermometer was then aligned with the work-piece by means of a He-Ne beam of the fibre laser as indicated in position 5 in Figure 4. Thereafter, the laser beam was switched on for the surface treatment to take place. The infra-red thermometer was then switched on shortly after and followed the laser ceramic interaction as the laser processing began. The infra-red thermometer was switched off before the fibre laser processing was completed (see Figure 4). This procedure was adopted for every measurement that was taken for the experiment which allowed an

average temperature to maintain closer to the real temperature of the processing area. However, it was important that the operator constantly monitored the processing area through the viewing window of the lens of the infra-red thermometer whereby the traversing laser beam was followed in order to accurately measure the temperature during the laser processing. The temperature measurement was conducted on five different areas of the surface of the ceramic work-piece as indicated in Figure 4. The measurement on the surface was conducted as the beam traversed on the surface of the work-piece. Each area was measured in one pass of the laser beam. Average was taken after all results were repeated x 5 on identical samples in order to produce consistency in the temperature reading.

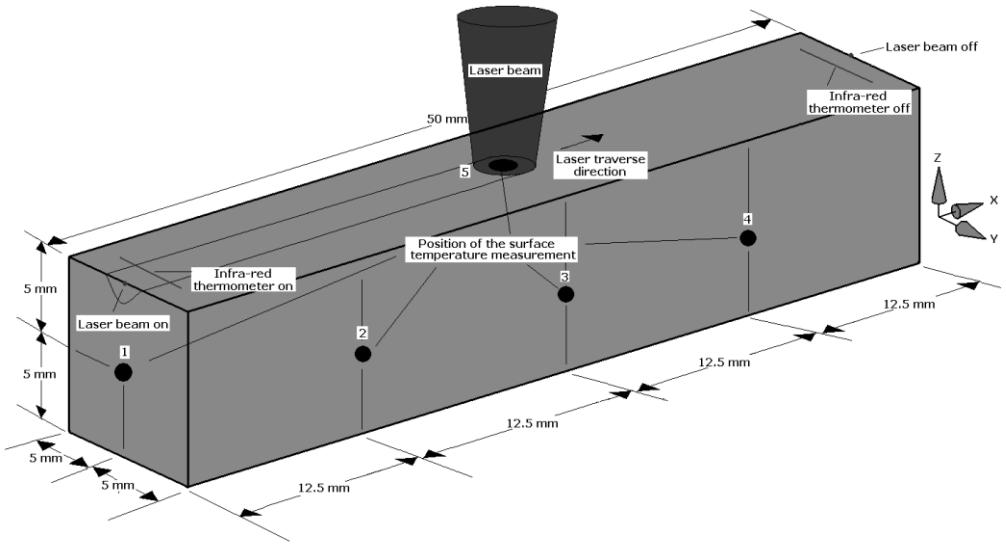

Figure 4 A schematic diagram of the positions used to measure the surface temperature of the Si_3N_4 engineering ceramic during the fibre laser processing.

3.3.2. Digital temperature reader

The bulk temperature measurement was taken using a precision fine wire (0.20 mm diameter x 152 mm in length), R-type, thermo-couples, capable of reading up to 2300°C (P13R, Omega Instruments Ltd) and were precisely mounted at various

positions within the bulk of the sample as illustrated in Figure 5. Each of the fine wire thermocouples set was wired to a two pin plug which connected to a digital temperature reader (N9002-Thermometer; Comark Ltd) for receiving the feedback in for of a temperature reading. Three holes were drilled into the ceramic using the ultrasonic drilling method, after which the tip of the thermocouples were mounted into the holes at 3, 6, 8 mm from the surface (see Figure 5). The holes were then filled using filler (paste) made of organic type material that is stable during high temperature processing. This assured firm fixation for the thermo-couples during the laser processing. Measurement was taken in three different passes of the laser treatment as one pass could only measure the temperature from a single set of thermocouple positioned in a single hole. A new sample was used with each pass of the fibre laser and five identical readings were recorded for each of the positioned hole to achieve consistency in the bulk temperature measurement.

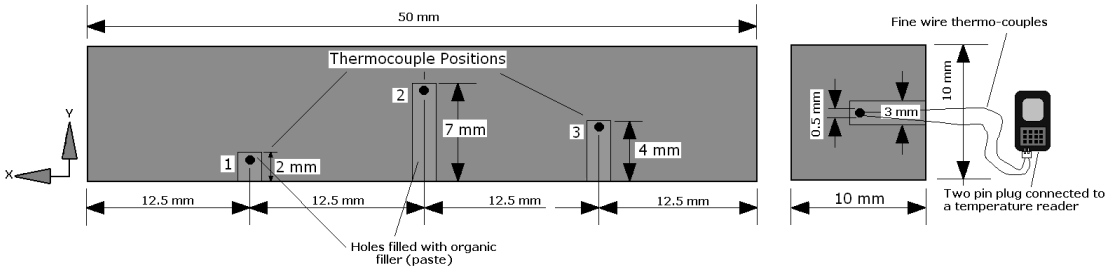

Figure 5 A schematic diagram of the mounting position of the thermo-couples into the Si_3N_4 engineering ceramic work-piece during the fibre laser surface radiation.

3.4. Thermogravimety-differential scanning calorimetry (TG-DSC) analysis

TG-DSC analysis (1500 DSC; Stanton Redcroft, Ltd.) was conducted on the as-received and fibre laser treated Si_3N_4 samples. The average surface area of the samples was approximately 2 mm^2 and the mass was 26 mg. The samples were placed into an Al_2O_3 crucible and N_2 was used as a purge gas at 50 ml/min. Once in place,

the samples were heated up to 1500 °C at a rate of 10 °C/min to measure the mass flow as the temperature increased. The samples were then cooled to ambient temperature at the same rate using the same parameters to measure the mass flow as the temperature reduced. The heat flow through the as-received and fibre laser treated samples was recorded for any changes during the heating and cooling cycles and is shown in Figure 15 and Figure 16. From this recording it was then possible to identify specific phase events that occur in the Si_3N_4 during heating at what temperature these events take place.

4. Results and Discussion

4.1. Experimental temperature readings

The average temperatures found on the surface of the Si_3N_4 ceramic after five passes of the fibre laser are presented in Figure 6(a); the surface temperature and in Figure 6(b); the bulk temperature of the Si_3N_4 ceramic. At the laser-ceramic interface the surface temperature was found to be 2269 °C. This was considerably higher than the melting general melting temperature of the ceramic (1900°C) [36] in comparison when the Si_3N_4 ceramic undergoes a decomposition phase. The difference between the two readings was 19.5%. This undoubtedly showed that the fibre laser processing temperature was sufficiently higher than that of the decomposition temperature of the Si_3N_4. This result complied with the finding of Shukla and Lawrence [30, 43] where it was shown that the laser surface treatment resulted to some degree of melting of the top (near) surface of the Si_3N_4 ceramic. The surface temperature on the side of the sample (away) from the laser treated zone was found to be much lower than the melting temperature which would obviously be high due to the heat transferring through the bulk of the ceramic. Interestingly, the temperatures reading should result

to being stable throughout one surface plane; however, this was not the case as the difference between position 2, 3 and 4 was sufficiently large as shown in Figure 6.

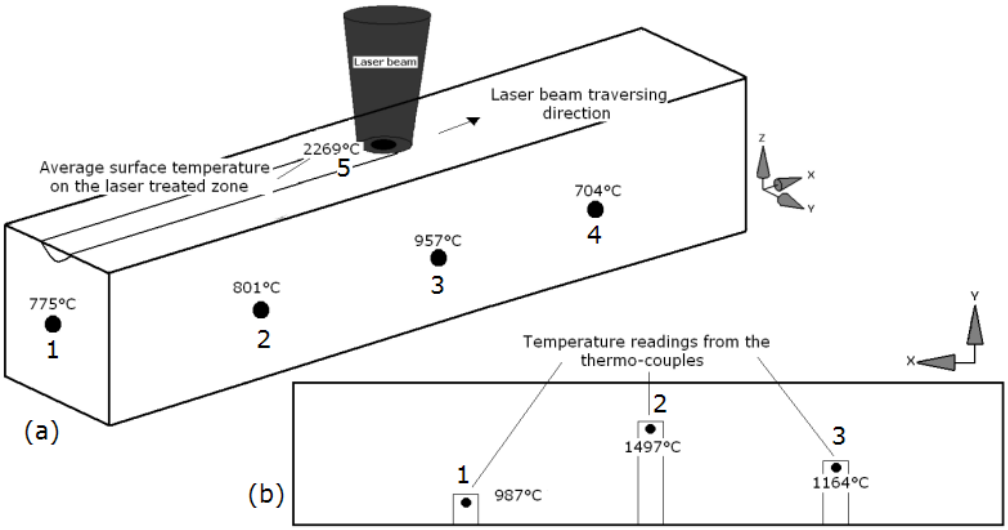

Figure 6 Schematic of the surface temperature reading in (a) and (b) the bulk temperature of the Si_3N_4 engineering ceramic.

The temperature measurements taken from using the thermo-couples within the bulk of the Si_3N_4 ceramic are presented in the Figure 6(b). The average bulk temperature after five readings in position 1, 2 and 3 (see Figure 5) were 986°C, 1497°C, and 1164°C was recorded. This result agrees with the surface temperature presented in Figure 6(a) that 3mm below the surface due to the heat transfer; the temperature is above 400°C lower. At 6mm below the surface, the measured temperature was considerably lower (1164°C). In this position, the temperature has begun to decrease as the heat was distributed throughout the surface. Moreover, the temperature at 8mm below the surface was 987°C as the heat was passed on from the bulk of the ceramic to the surface.

In Figure 7(a) and (b), both of the graphs are constructed from the experimental values found. This was for a situation where the fibre laser was incident at 25 mm length (centre) from the edge of the Si_3N_4 ceramic. The distribution of heat is

presented in Figure 7(a), which illustrates the surface temperature over the length of the Si_3N_4 sample at 25 mm. At the length of 0 mm the experimental temperature was instantaneously ramped to just under 800 °C and gradually increases as it come closer to the incident beam. The peak temperature found was 2269°C at 25 mm length (centre of the work-piece) of the focused laser beam upon the Si_3N_4 test piece. The temperature reduced to 730°C at 37.5 mm in length and was recorded at 750°C at the edge of the sample at 50 mm.

The graph in Figure 7(b) presents the experimental temperatures obtained in the bulk of the ceramic particularly at 1, 2 and 3 mm (see Figure 7(b)). Temperatures at various other positions can also be calculated from these three values as shown in Figure 7(b). In general the curve in Figure 7(b) has declined due to the reduction of the temperature through the bulk of the ceramic. The temperature is reduced from 2269°C at the depth of 0 mm (surface) to 1500°C at 3 mm, 1235°C at 6 mm and 1195°C at 8 mm depth. From this; the temperature at the depth of 10 mm can be predicted as shown in Figure 7(b).The experimental investigation would now be used as a base to construct the FEM. The results found herein are also compared to the FEM for validation and confirmation of the level of accuracy or error in the temperature measurements in this study.

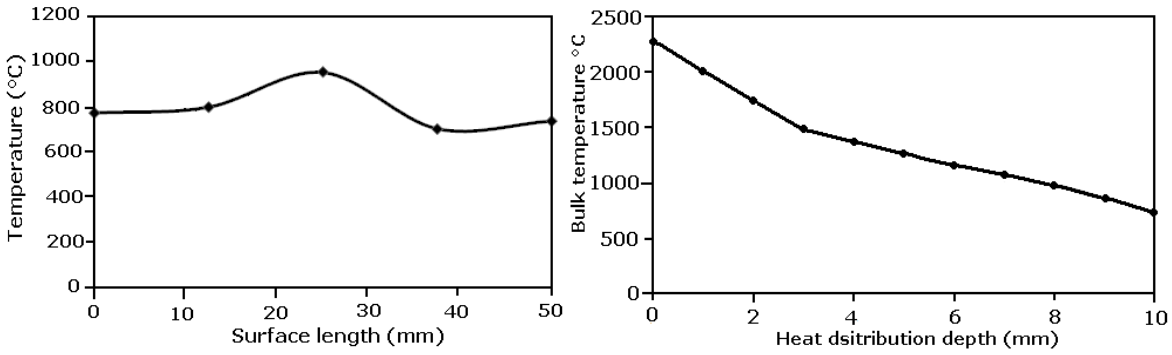

(a) **(b)**

Figure 7 Experimental temperature distribution over the surface length in (a) and (b) the temperature distribution through the bulk of the fibre laser processed Si_3N_4 engineering ceramic.

4.2. FEM temperature reading

A FEM was constructed which revealed the surface and the bulk temperature maps by taking in account of the surface and the bulk temperatures measured from the experimentation. The surface maps are presented in Figure 8, 10 and 12. Because of the laser beam traversing as a CW beam; it is always ideal to construct the model so that it illustrates the FEA of a moving laser beam. However, in this case, a stationary spot was used for the analysis to observe the thermal radiation. The total time to cover the whole area of the sample was 30 sec at a traverse speed of 100 mm/min which would cover 1.66 mm/sec. In Figure 7; the first point of contact with the ceramic and the laser beam has been demonstrated. The impact on the beam is only 1.5 mm onto the surface despite comprising of a spot size of 3 mm diameter. A heat map is illustrated for this condition and is compared with the values for the experimental temperature readings that were found. It can be observed that the maximum temperature found at the laser-material interface on the FEM was 2236°C. The temperature here was lower than the temperature from the real experimental value by only 1.5%. Error of the computational method within 10% can be considered to be in good agreement with the experimental values. In Figure 8(b); the laser beam is only concentrated at 50% of its diameter because it is focused on the edge of the sample (start of the laser treatment process), which enabled the cross-sectional distribution of heat to be analysed. From observing the cross-sectional heat map, it can be seen that the near to melting temperature found through the bulk of the ceramic

ranges between 100 to 200µm. This reading complied with the result of previous investigations where, a degree of surface melting and decomposition has been found by Shukla and Lawrence [33].

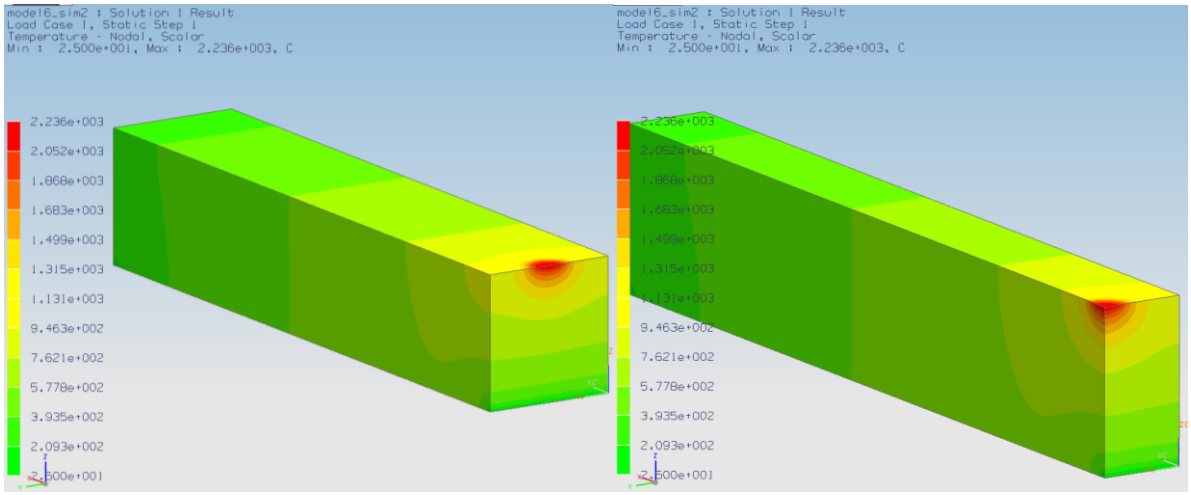

Figure 8 FEM of the heat distribution of the fibre laser focused at 0mm from the edge (position 1) of the Si_3N_4 ceramic work-piece (start of the laser treatment) in (a) and (b); the cross-sectional view.

From observing the results from the model in Figure 8(a) and (b), the determination of temperature distribution over the surface at various lengths and through the bulk at various depths are presented in the graph in Figure 9(a) and Figure 9(b). In this model, the incident beam at the start of the surface treatment is covering 0 to 1.5 mm radius. The temperature within this area as seen on Figure 9(a) is up to 2228°C. During this time the temperature distribution over the rest of the surface is lower. This is due to the heat transfer taking effect over the surface. At 25 mm in the centre of the work-piece, the temperature was up to 583°C and at 50 mm (edge of the sample); the temperature was much lower. The result of the FEM at this position appears to be in good agreement with that of the experimental result. However, from observing the depth of the distribution from the model in Figure 9(b); the surface temperature at 0 mm is 2250°C and reduces to

790°C at the depth of 2mm, 650°C at 4 mm, 480°C at 7mm and finally reducing to 25°C at 10 mm (room temperature).

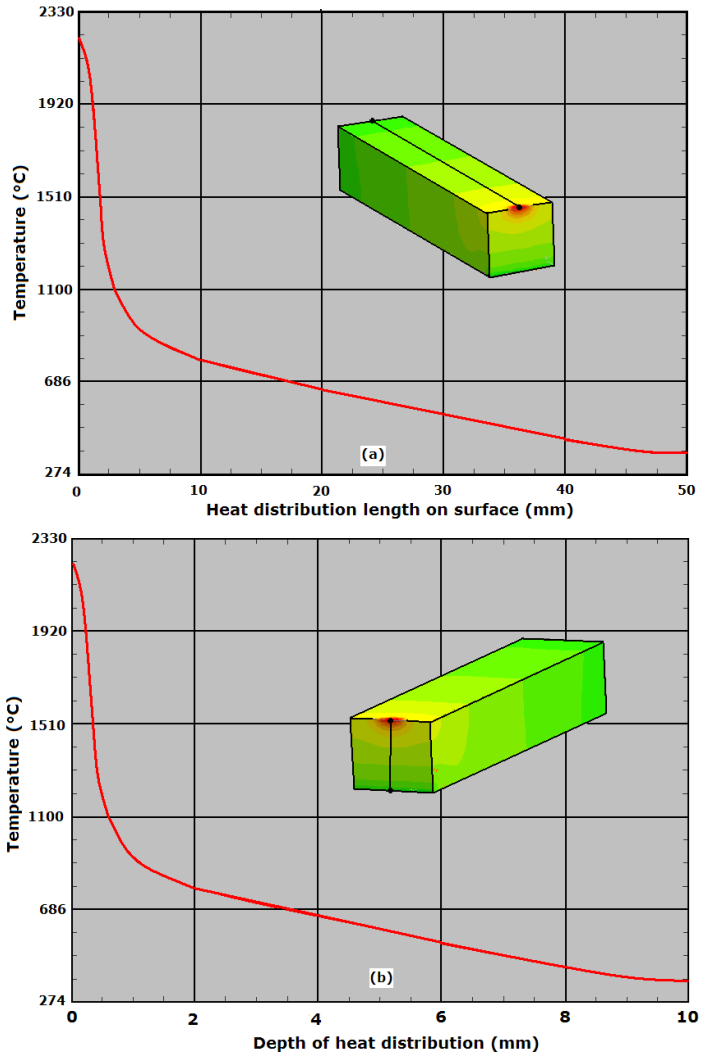

Figure 9 Temperature curves from the FEM of the initial stage at 0 mm from the edge (position 1) of the fibre laser irradiation of the Si_3N_4 ceramic for (a) the heat distributed over the length of the sample and (b) the heat distribution through the depth of the sample.

The FEM in Figure 10(a - c) showed that the temperature pattern was somewhat different to that of the one found at the start of the laser treatment (see Figure 8 and Figure 9) as the average heat input began to increase over the total surface area of the Si_3N_4 ceramic. Despite the decomposition and surface melting arising during the laser interaction and the

rapid cooling effect taking place; the temperature at the laser radiated zone has increased on the surface and through the bulk as presented in the graph in Figure 11.

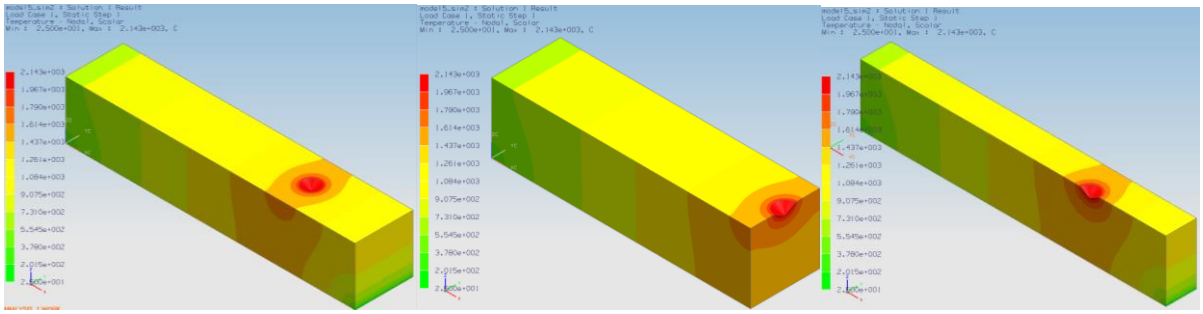

Figure 10: Figure 10: FEM of the heat distribution of the fibre laser focused at 12.5mm from the edge (position 2) of the Si_3N_4 ceramic work-piece in (a) and the cross-sectional view in (b) and (c).

The traversing laser beam is paused in time at 12.5 mm from the edge in order to show the effects at that position. At 12.5 mm the highest temperature on the surface was found to be 2143°C (see Figure 11). Gradually, the temperature begins to decrease to 1168°C at 25mm, 953°C at 37.5 mm and 729°C at 50 mm. The temperature through the bulk has increased in comparison with the bulk temperature during the start of the fibre laser treatment due to the increased in time that the laser beam has spent on the ceramic which would have caused a sufficient level of heat to be produced. From melting temperatures at 0 mm on the surface; the temperature reduces to 1355°C through the bulk at the bottom surface layer as the heat is passed on, during the laser-ceramic interaction at 12.5 mm in length after the start of the treatment.

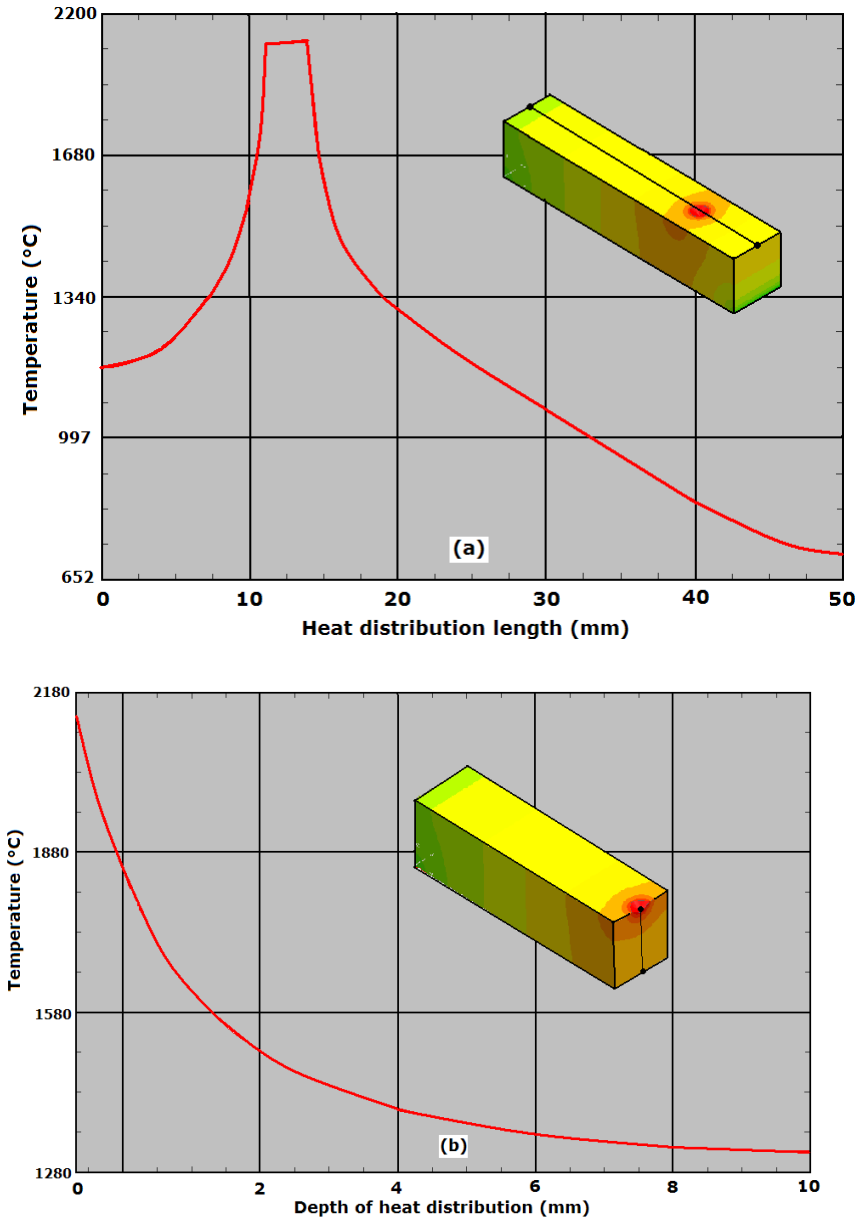

Figure 11 Temperature curves from the FEM of the fibre laser irradiation at 25 mm from the edge (position 3) of the Si_3N_4 ceramic for (a) the heat distributed over the length of the sample and (b) the heat distribution through the depth of the sample.

The illustrations in Figure 12(a), (b) and (c) show the FEM of the laser-ceramic interaction in the centre of the work-piece (25 mm from the edge). In this position the distribution of heat is different to the interaction during the initial stages as previously shown. The Si_3N_4 ceramic in this position is in thermal equilibrium since the temperature

distribution is well balanced. At 25 mm the heat is at its peak (2287°C) near to the melting temperature of the Si_3N_4 ceramic. During this time, the temperature slope gradually increases to the highest position as shown in Figure 13(a) and maintains for 3 mm and then declines and has the opposite effect where the temperature is curve is declined.

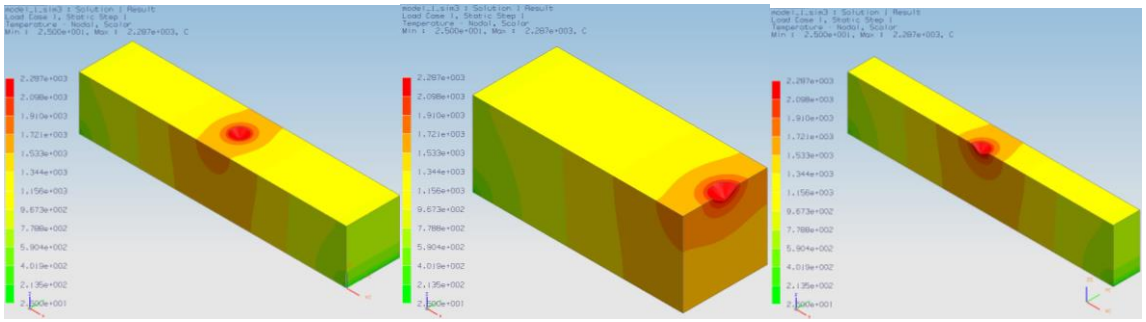

Figure 12 FEM of the heat distribution of the fibre laser beam focused in the centre (position 3) of the Si_3N_4 ceramic work-piece in (a) and in the cross-section in (b) and (c).

From this point onwards; as the laser beam traverses furthermore on to the sample, the effect of heat distribution is similar to that of the one presented in previous FEM's. The temperature distribution over the surface was similar to that of the FEM presented in Figure 10 as well as the results obtained from the experimental model. The difference between the experimental model and the computational FEM in was less than 1 % particularly for the temperature predictions over the surface length. The bulk readings for the two compared models were also in good agreement. However, consideration should be given to the accuracy of thermometer device used for measuring the experimental temperature (±10%) as well as the distance which the temperature measurement was taken from as these factors will have a considerable effect on the experimental readings. The distance of the temperature measurement changes as the laser beam traverses away from the focused infra-red beam of the thermometer device (see Figure 3) which would also cause some fluctuation in the results found.

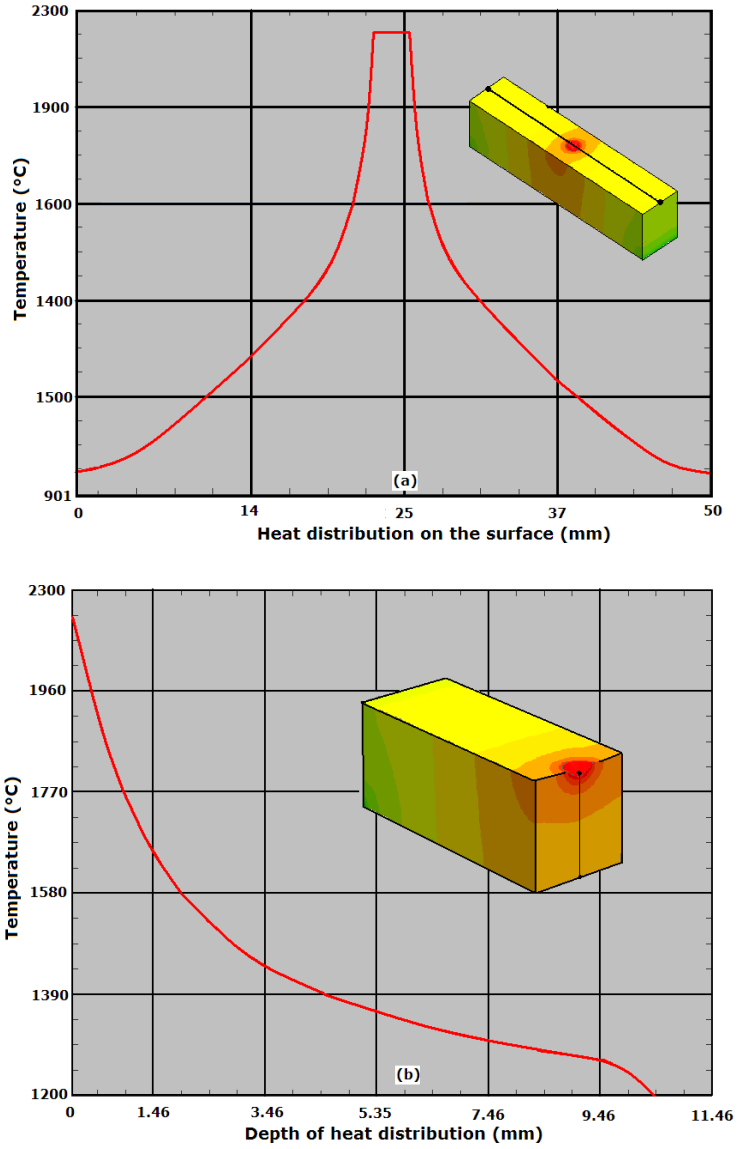

Figure 13 Temperature curves from the FEM of the fibre laser irradiation at 25 mm from the edge (position 3) of the Si_3N_4 ceramic for (a) the heat distributed over the length of the sample and (b) the heat distribution through the depth of the sample.

4.2. Comparison of the experimental and the FEM

At the laser-ceramic interface the surface temperature was found to be 2269°C (see Figure 6). This result is in good agreement with that of a previous investigation Shukla and Lawrence [34], where it was found that fibre laser surface treatment of the Si_3N_4 resulted in some degree of decomposition as the temperatures were reached over its melting point on of the top

(near) surface layer. Interestingly, the temperature readings would be expected to be stable throughout a plane, but this was not the case as up to 36% difference in temperatures between Positions 2 to 3 and 4 to 5 was observed. The difference between the two results may have resulted from the error in reading the temperature resulting from the contact-less infra-red thermometer device, fluctuation in the laser power during the processing stage (although, stable output powers were recorded prior to the laser treatment) and the ceramic material being somewhat inhomogeneous.

The temperature is expected to be fairly high in at the edges of the samples in position 5 and on the same surface plane in position 2, 3, and 4 as it is at the edge of the sample indicating that there is less area for the heat to travel which created sufficient heat at the surface. Still, the experimental surface temperature measurements agree with those of the FEA model (reference to Figure 12) less than +10% error. Further modification to the temperature measurement settings would improve the consistency in obtaining more accurate temperature readings.

The average temperatures measured within the bulk of the Si_3N_4 after five readings also agree with the bulk temperatures predicted by the FEA model. At 3 mm below the surface the temperature was up to 1525°C. The FEM by comparison gave a temperature of over 1460°C, and agreement of just under 5 %. The temperature in Position 3 (see Figure 6 (b)) was found to be 1164°C which in comparison to the FEM was 169°C lower, indicating an error of 14%. Finally, at Position 1 in Figure 6(b) the temperature recorded was 987°C, while the temperature predicted by the FEM model was 1275°C, a difference of 29%. It is clear that the temperature predictions by the FEM were slightly higher than expected in comparison to those obtained by experimental means. This may have resulted due to factors such heat loss through the 3 mm holes drilled into the sample, lack of contact of the thermocouples to the

material surface and the thermocouple response time. Such aspects were not taken into account by the FEA model and so the FEA results will always be higher.

4.3. Development of extended parameters from the FEM

Range of possibilities can be accrued based on the results obtained from the FEM for parameters such as traverse speed; power density; depth of heat distribution; temperature; and time, in relationship to one another. Based on this, prediction of the input parameters during fibre laser surface treatment of the Si_3N_4 ceramic at various input parameters (see Figure 14 (a-g)) can be made. As with all laser processes, the results herein show that a lower traverse speed at high power density would generate high processing temperatures. This inherently, would produce deeper distribution of the thermal energy; the effects are opposite when the processing speeds increases or the power density decreases. This is when the surface temperature is also reduced with lower penetration of the thermal energy into the bulk of the ceramic. Consideration of power density would also allow one to gauge the effect of the laser spot size as an additional parameter, since the spot is a function of the power density applied. Typically, a smaller spot size than 3mm by using the same power input (143.25 W) would produce a much bigger power density and would further compliment the model that are presented in this study.

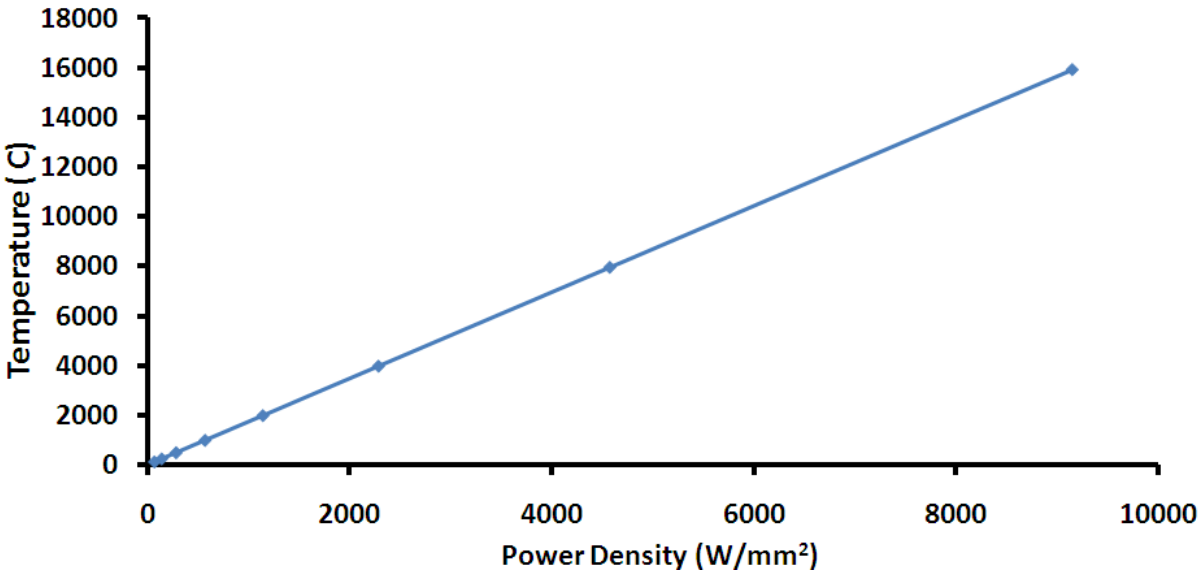
18000
16000
14000
12000
10000
8000
6000
4000
2000
0
Temperature (C)
0
2000
4000
6000
8000
10000
Power Density (W/mm²)

(a)

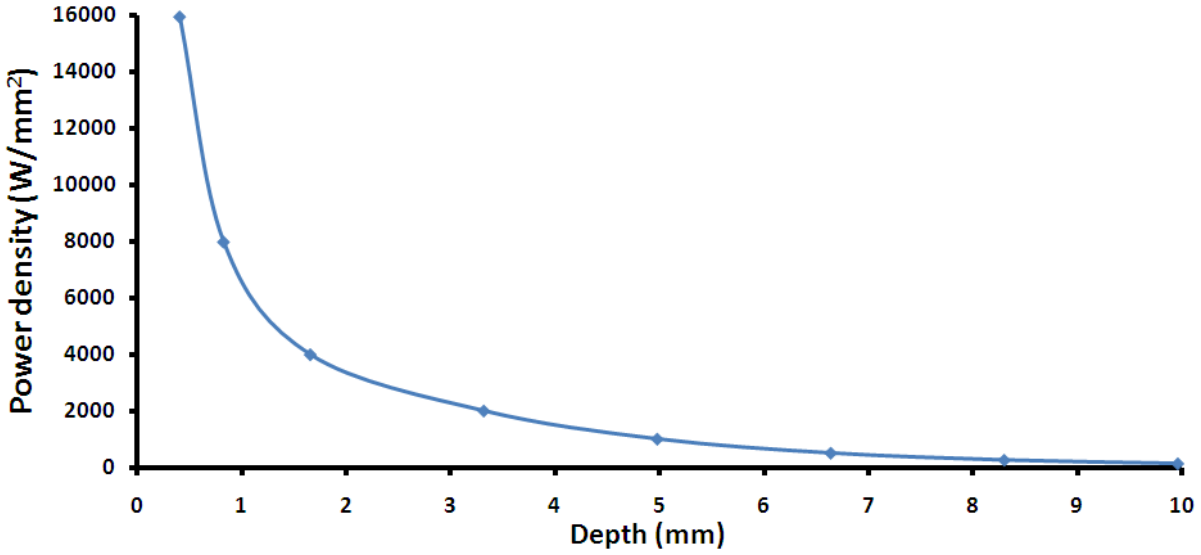
16000
14000
12000
10000
8000
6000
4000
2000
0
Power density (W/mm²)
0
1
2
3
4
5
6
7
8
9
10
Depth (mm)

(b)

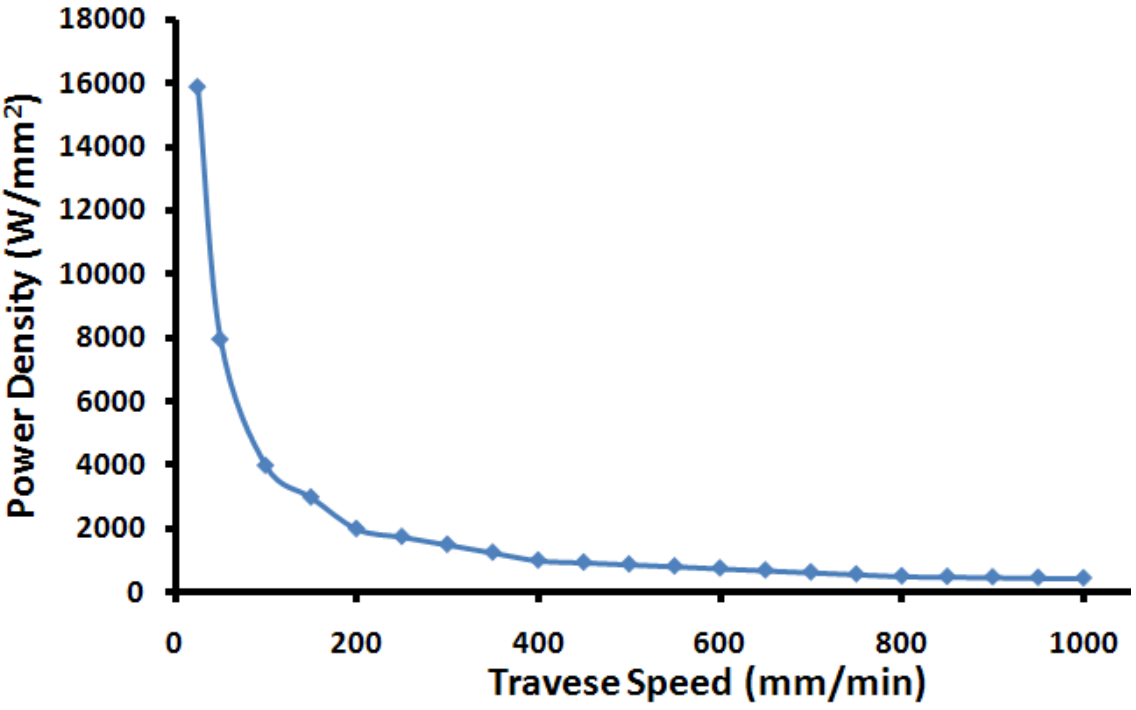
Power Density (W/mm²)
18000
16000
14000
12000
10000
8000
6000
4000
2000
0
0
200
400
600
800
1000
Travese Speed (mm/min)

(c)

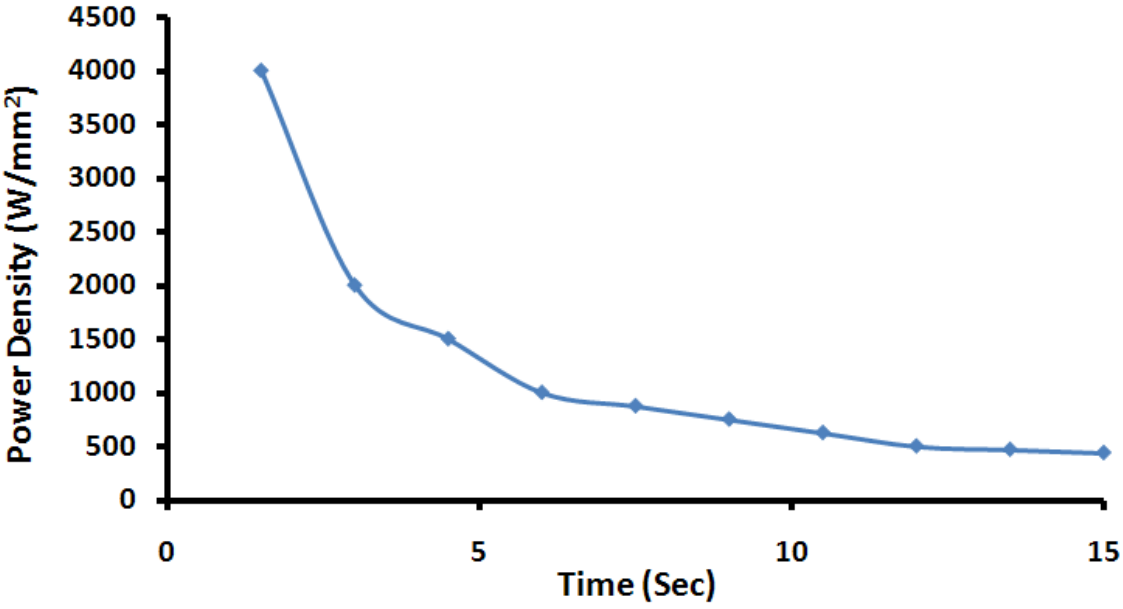
Power Density (W/mm²)
4500
4000
3500
3000
2500
2000
1500
1000
500
0
0
5
10
15
Time (Sec)

(d)

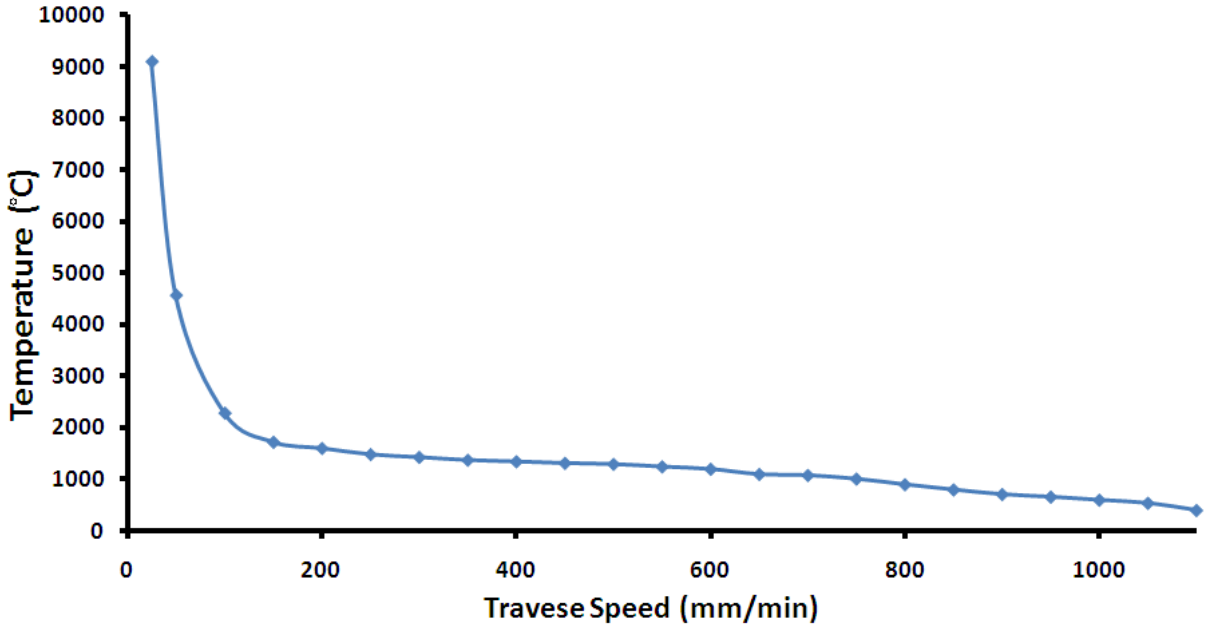
Temperature (°C)
10000
9000
8000
7000
6000
5000
4000
3000
2000
1000
0
0
200
400
600
800
1000
Travese Speed (mm/min)

(e)

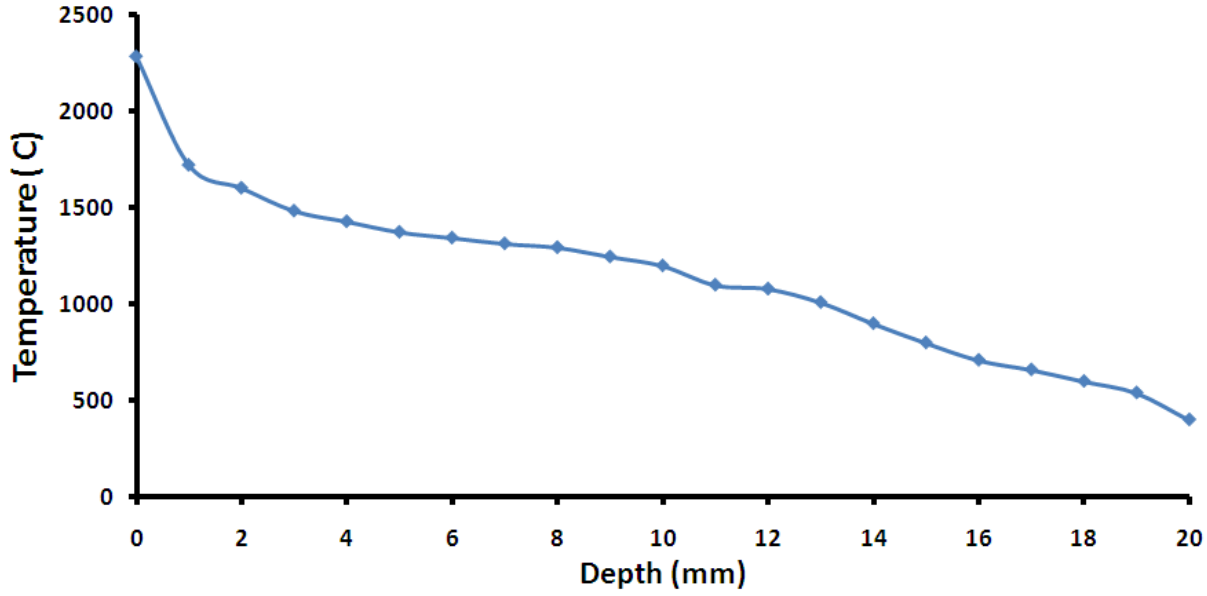
Temperature (C)
2500
2000
1500
1000
500
0
0
2
4
6
8
10
12
14
16
18
20
Depth (mm)

(f)

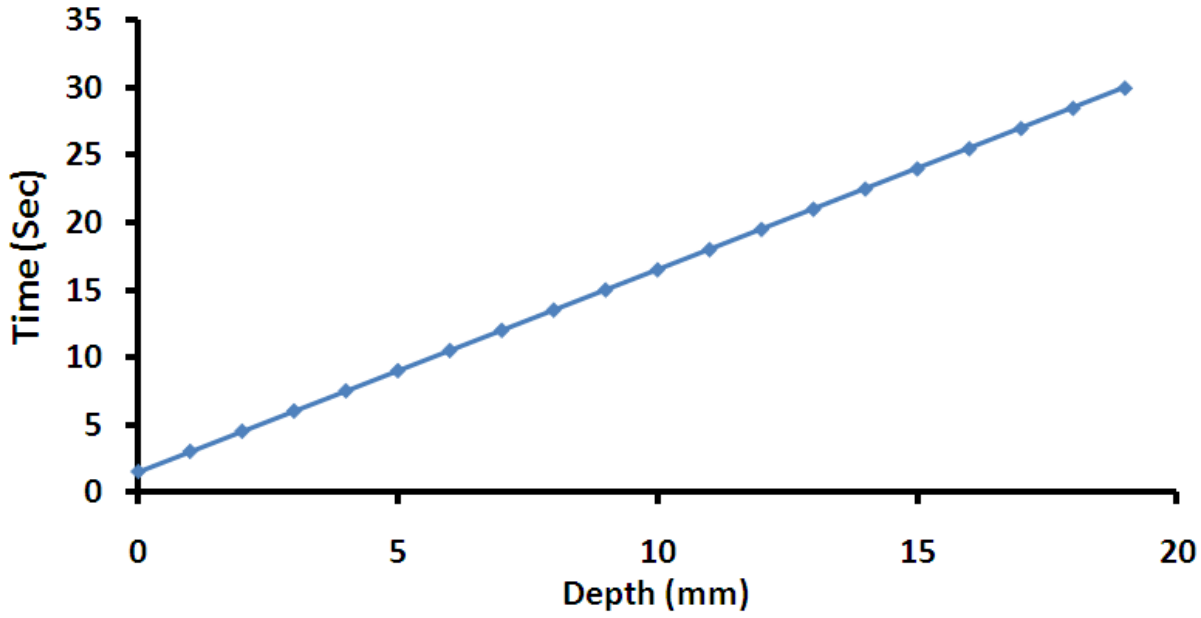

(g)

Figure 14 Parameters obtained from the FEM showing the coloration of various parameters with one another; (a) power density Vs temperature; (b) depth Vs power density; (c) power density Vs traverse speed; (d) power density Vs time; (e) traverse speed Vs temperature; (f) depth Vs temperature and (g) depth Vs time for fibre laser processing of the Si_3N_4 engineering ceramic.

5.0. Phase transformation

Figure 15 and Figure 16 show the changes in within the Si_3N_4 engineering ceramic after heating to 1500 °C and cooling to room temperature during the TG-DSC analysis. Figure 15 represents the as-received surface and Figure 16 illustrates the fibre laser radiated surface. As one can see, there is a considerable difference in the events which have occurred for the two samples. The fibre laser radiated surface in comparison to the as-received surface has allowed much more mass flow to have occurred. The highest mass flow found on the fibre laser radiated surface was about 270 mW when compared to the as-received surface which was about 37 mW. This would have occurred from the heat induced by the fibre laser radiation which in turn caused some degree of densification of the Si_3N_4 ceramic which intrinsically

allowed more heat to flow through the bulk due to air blocks or cavities within the as-received sample, which would in turn cause a decline in the mass.

At 50 °C, a rapid decline in the heating curve can be seen which indicate an endothermic reaction as the Si_3N_4 would have began to absorb the atmospheric gases and had began the process of oxidation which would last over the full course of heating the sample to high temperatures. Evidence of some change was also observed from the curve between 1300 °C to 1450 °C. From this, it can be postulated that the phase transformation of the Si_3N_4 engineering ceramic has started to take place where large percent of the α-phase is present and the β-phase has began to form. At 1400 °C the transition between α-phase to β-phase would have occurred where $\alpha+\beta$ would be found. The gradient of the curve begins to increase beyond 1400 °C which presents the increase in the mass flow and indicate the end of the phase transformation where main the β-phase is evident. Beyond 1450 °C, the Si_3N_4 engineering ceramic has fully transformed to β-phase and shows the end of the phase transformation. At 1500 °C the cooling cycle begins where it can be seen that the cooling curve has lower mass flow on average and almost identical events occurring. When the sample was cooled it can be seen that the mass flow was slightly lower and the decline in the curve found at about 1400 °C was not to be observed during the cooling stage. This was because the Si_3N_4 engineering ceramic does not usually have the tendency to produce reverse phase transformation as stated by Messier *et al*. [23]. The TG-DSC analysis was only performed from room temperature to 1500 °C which demonstrated the expected changes that have occurred, although, postulation can be made for the events which take place after the 1500 °C since the temperature found both in the FEM and the experiments model up to 2200 °C which indicate that decomposition and melting would occur around 1900 °C.

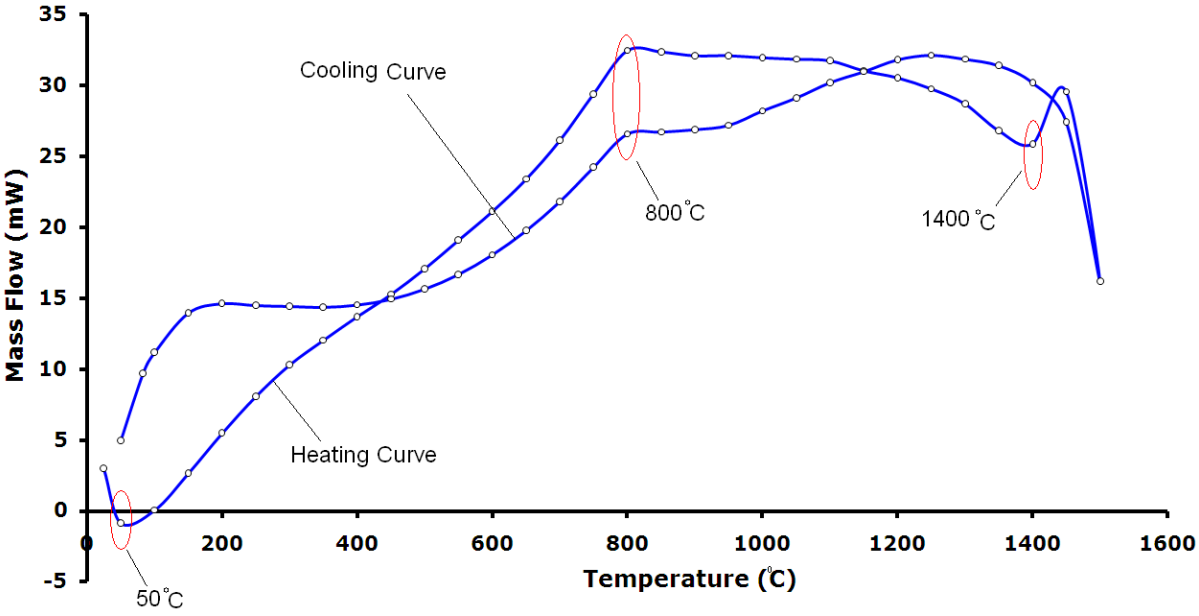

Figure 15 Heating and cooling curve from the TG-DSC analysis for the as-received surface of the Si_3N_4 engineering ceramic.

The TG-DSC curve for the fibre laser radiated surface was somewhat different in comparison to that of the as-received surface as mentioned previously. This was because the fibre laser radiation has produced a change in composition of the sample which was considerable different to that of the as-received sample. This change has been presented in an earlier publication by Shukla and Lawrence [30] which demonstrated the formation of the SiO_2 layer formed on the Si_3N_4 ceramic. Therefore, the oxidized surface did not show any evidence of major change during the TG-DSC analysis as there was considerable amount of change had taken place already from the fibre laser radiation. From analysing event which has taken place during the TG-DSC analysis of the fibre laser radiation of the as-received sample, it can be said that the α-phase to β-phase transformation has already occurred within this during the fibre laser treatment possible between 1300 °C to 1450 °C which then was irreversible during the cooling stage. The presence of the β-phase can be confirmed by comparing the SEM image of the fibre laser radiated surface presented in Figure 17(a) and comparing it with the

as-received surface of the Si_3N_4 in Figure 17(b) where it is evident that change in morphology and the micro-structure by elongated rod-like grains in large numbers as well as the formation of the SiO_2 zones can be found on the fibre laser radiated surface in Figure 17(b). This type of behaviour was also mentioned by the work of Sarin [22], Messier *et al.* [23], Ziegler and Hasselman [24] and Dai *et al.* [28] who investigated the phase transformation of the Si_3N_4 ceramic during its exposure to high temperature gradients.

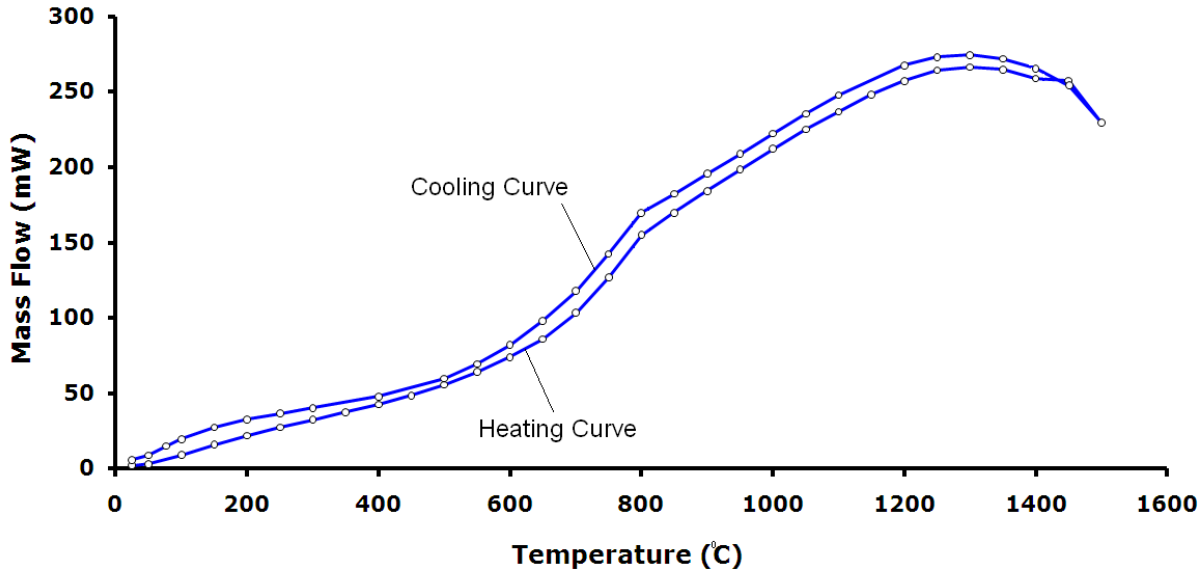

Figure 16 Heating and cooling curves from the TG-DSC analysis for the fibre laser radiated Si_3N_4 engineering ceramic.

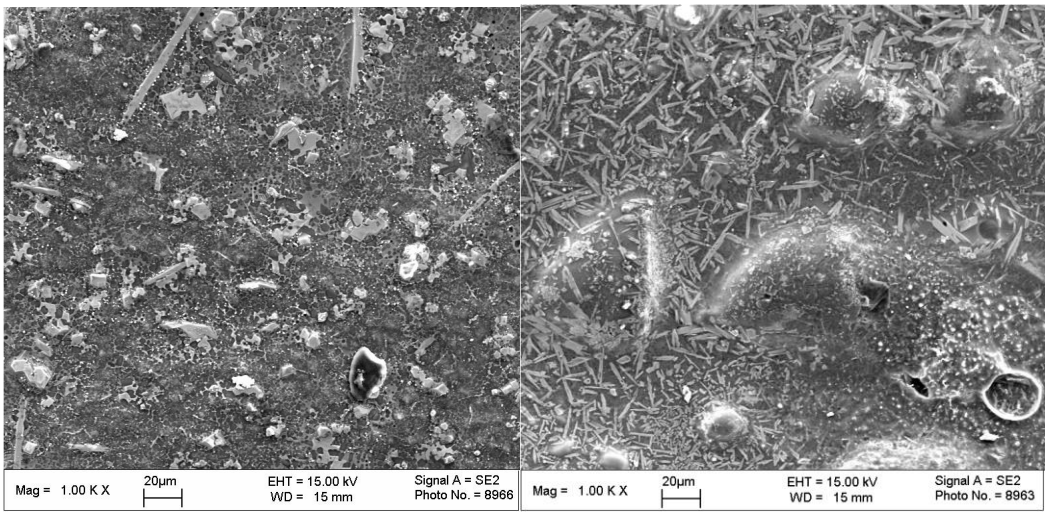

(a) (b)

Figure 17 SEM image of (a) the as-received surface and (b) the fibre laser radiated surface of the Si_3N_4 engineering ceramic.

6.0. Conclusions

The thermal effects of the fibre laser surface treatment of a Si_3N_4 engineering ceramic were modelled using an experimental model and FEM. The temperature analysis from both of the models was used to map phase changes within the Si_3N_4 engineering ceramic which all led to form the following conclusions:

- From both surface and the bulk temperature measurements the distribution of the temperature over the length and the depth of a Si_3N_4 engineering ceramic sample during the fibre laser surface treatment was also presented and the FEA model and was verified with an overall accuracy of +10%.

- This is consistent over estimate of temperature by the FEA model may have resulted due to: (a) heat loss through the 3 mm holes drilled into the sample; (b) lack of contact of the thermocouples to the material surface and (c) the thermocouple response time. Such aspects were not taken in account by the FEA model and so the FEA results will always be higher. Furthermore, the FEA model expanded to show the relationship between the processing temperatures, time and the depth of heat distribution with parameters such as the traverse speed and power density which when correlation with one another revealed the extended range of parameter window during the fibre laser surface processing of the Si_3N_4 engineering ceramic.

- Data obtained from a thermogravimetry-differential scanning calorimetry (TG-DSC) analysis and the FEA model predictions was used to map the phase transformations in the Si_3N_4 resulting from fibre laser surface treatment. The mapping revealed that the

fibre laser surface treatment generally resulted in a phase transformation of the Si_3N_4 from α-phase to β-phase.

- The phase transformation begins to occur at 1300 °C and ends at round 1400 °C where a mixture of α-phase and β-phase ($\alpha \rightarrow \alpha + \beta$) is found which then transforms to $\alpha + \beta$ at about 1400 °C and fully transforms from $\alpha + \beta \rightarrow \beta$-phase at 1450 °C.

- During this stage densification of the ceramic occur and further results to a change in the micro-structure of the Si_3N_4 as evidence of elongated rod-like grains as well as formation of SiO_2 can be evident on some regions of the fibre laser radiated surface.

6. References

1. J. Cline, T R Anthony, Heat treating and melting materials with a scanning laser beam. Journal of applied physics. 48 (1977) 3895- 3900.

2. M. Lax, Temperature rise induced by a laser beam. Journal of applied physics. 48 (1977) 3919 - 3924.

3. M. Lax, Temperature rise induced by a laser beam II. The nonlinear case Journal of applied physics 33 (1978) 1127-1129.

4. Y. I. Nissim, A. Lietoila, R.B. Gold, J.F.R. Gibons, Temperature distributions produced in semiconductors by a scanning elliptical or circular CW laser beam. Journal Applied Physics. 51 (1980) 274-279.

5. J.E. Moody and R.H. Hendel, Temperature profiles found by a scanning laser beam. Journal Applied Physics. 53 (1982) 4364 – 4371.

6. A. Kar, and J. Mazumber, Three-dimensional transient thermal analysis for laser chemical vapour deposition on uniformly moving finite slabs. Journal of applied physics. 65 (1989) 2923 – 2934.

7. A. Kar, Effects of mode structure on three-dimensional laser heating due to single or multiple rectangular laser beams. Journal applied physics. 80 (1996) 667 – 674.

8. Z. Zhang and M.F. Modest, M. F, Temperature dependent Absorptances of ceramics for Nd:YAG and CO_2 laser processing Applications. Journal of heat Transfer. 120 (1998) 322 -327.

9. L. Hao, and J. Lawrence, Numerical modeling of the laser surface processing of magnesia partially stabilized Zirconia by the means of three-dimensional transient finite element analysis. Proceedings of the Royal Society A. 462 **(no 2065),** (2006) 43-57.

10. M.B. Ignatiev, Yu.I. Smurov, G. Flamant, and V.N. Senchenko, Surface temperature measurement during pulsed laser action on metallic and ceramic materials. Journal of applied surface science. 96-98 (1996) 505 -512.

11. W. Braisted, and R. Brockman, Finite Element Simulation of laser shock peening. International journal of fatigue. 21 (1998) 719 – 724.

12. Hu. Yongxiang, Yao, Zhenqiang and Hu. Jun, 3-D FEM Simulation of laser Shock Processing. Surface and Coating Technology. 21 Issue 3-4 (2006) 1426 – 1435.

13. J.L. Ocana, M. Morales, C. Molpeceres, J. Torres, Numerical simulation of surface deformation and residual stresses fields in laser shock processing experiments. Journal of applied surface science. 238 (2004) 224 – 248.

14. H. Chen, J.W. Kysar and Y. Y. Lawrence, Characterization of plastic deformation induced by micro-scale laser shock Peening. Journal of applied mechanics (ASME). 71 (2004) 713- 723.

15. M. J. Kim, 3-D Finite element analysis of evaporative Laser cutting. Applied mathematical Modelling. 29 (2005) 938 – 954.

16. M. Shiomi, A. Yoshidome, F. Abe, K. Osakada, Finite element analysis of melting and solidifying processes in laser rapid prototyping of metallic powders. International Journal of Machine tools and manufacture. 39 (1998) 237 – 252.

17. C. Carmingnani, R. Meres, G. Toselli, Transient finite element analysis of deep penetration laser welding process in single pass butt-welded, thick steel plate. Computer methods in applied mechanics and engineering. 179 (1999) 197- 214.

18. R. Spina, L. Tricarico, G. Basile, T. Sibilano, Thermo- mechanical modelling of laser welding of AA5083 sheets. Journal of material process technology. 191 (2007) 215 – 219.

19. B. S. Yilbas, A. F. M. Arif, B. J. Abdul Aleem, Laser welding of low carbon steel and thermal stress analysis. Optics & Laser technology. 42 (2009) 760 – 768.

20. M. Zain-Ul-Abdein, D. Nélias, J. F. Jullien, D. Deloison, Thermo-mechanical Analysis of Laser Beam Welding of Thin Plate with Complex Boundary Conditions. International journal of material forming. 1 (2008) 1063- 1066.

21. Naeem, Dar. Ullah, M. E. Qureshi, M. Hammouda, Analysis of weld-induced residual stresses and distortions in thin-walled cylinders. Journal of mechanical science and technology 23 (2009) 1118-113.

22. V.K. Sarin, On the α-to-β Phase Transformation in Silicon nitride*, Material Science and Engineering, A105-106 (1981) 151-159

23. D. R. Messier, F. L. Riley, R. J. Brook, The α/β silicon nitride phase Transformation, Journal of Material Science. 13 (1978) 1199 – 1205.

24. G.Ziegler and D.P.H Hasselman, Effect of phase composition and microstructure on the thermal diffusivity of Silicon Nitride, Journal Material Science. 16 (1981) 495 – 503.

25. P.Sajgalik, D. Galisek, α/β Phase transformation of silicon nitride: homogeneous and heterogeneous nucleation, Journal of material science letters. 12 (1993) 1937-1929.

26. T. Rouxel, F. Rossignol, J.L Besson, and P. Goursat, Superplastic forming of α-phase rich silicon nitride, Journal of Material Research. 12, No.2 (1996) 480-492.

27. H Yang, G Yang, R Yuan, Densification and α-β phase transformation of Si_3N_4 containing MgO and CeO_2 during sintering, Materials Chemistry and Physics. 55 (1998) 164 – 166.

28. J. Dai, J. Li, Y. Chen, The phase transformation behaviour of Si_3N_4 with Re2O3 (Re=Ce, Nd, Sm, Eu, Gd, Dy, Er, Yb) additives, Material Chemistry and physics. 80 (2003) 256 – 359.

29. J Z Jiang, F Kragh, D J Frost, K Ståhl and H Lindelov, Hardness and thermal stability of cubic silicon nitride, Journal of Physics Condensed Matter. 13 No 22 (2001) L515 – L520.

30. P.P.Shukla J. Lawrence, Surface Characterization and Compositional evaluation of a fibre laser processed Silicon Nitride (Si_3N_4) Engineering ceramics, Laser in Engineering. (2010) in press.

31. T. Sham, NX 5.0 for designers. Purdue University Calumet. CADCIM Technologies, USA, 2007

32. W. D. Rolph, K. J. Bathe, An efficient algorithm for analysis of non-linear heat transfer with phase changes. International journal of numerical methods in engineering. 18 (1882) 119 – 134.

33. P.P. Shukla, and J. Lawrence, Characterization and compositional Evaluation of Engineering ceramic. Proceedings of ICALEO (2009) Orlando, FL.

34. P.P. Shukla, J. Lawrence, and H. Wu, On the Fracture Toughness of a Zirconia Engineering Ceramic and the Effects thereon of surface processing with fibre laser radiation. Proceedings of the Institution of Mechanical Engineers, Part B. Journal of Engineering Manufacture. (2009) in press.

35. A.Y. Cengel, R.H. Turner, Fundamentals of thermal fluid sciences, International edition, Mc Graw Hill: Singapore, 2001

36. Cambrige Engineering Material Selector (2008).